RESEARCH ARTICLE `OPEN ACCESS`

A Novel Impedance Platform Based on Printed Polymer Electrodes for Automated Virus Neutralization Assays

Stefanie Michaelis[1] | Anja Germann[2] | Marcus Schäfer[3] | Jannik Jungmann[4] | Anne-Kathrin Mildner[5] | Iris Riemann[2] | Saskia Bast[5] | Thorsten Knoll[2] | Sylvia Wagner[2] | Eike Kottkamp[4] | Daniel Baasner[4] | Boris Anczykowski[3] | Joachim Wegener[1,5] [ID]

[1]Fraunhofer EMFT, Fraunhofer Institute for Electronic Microsystems and Solid State Technologies, Regensburg, Germany | [2]Fraunhofer IBMT, Fraunhofer Institute for Biomedical Engineering, Sulzbach, Germany | [3]nanoAnalytics GmbH, Münster, Germany | [4]innoMe GmbH, Espelkamp, Germany | [5]Institute of Analytical Chemistry, Chemo- and Biosensors, University of Regensburg, Regensburg, Germany

Correspondence: Joachim Wegener (Joachim.Wegener@ur.de)

ABSTRACT

Cell-based neutralization assays are of central importance for the development of new vaccine candidates as well as quality assurance of already approved vaccines. Suppression of viral infection by neutralizing antibodies present in serum of vaccinated individuals serves as an indicator for efficacy of a vaccine. Established readouts used to date are hardly automated, provide no time resolution and require expensive reagents. These shortcomings are limiting factors in vaccine development. In contrast, when virus-compatible host cells are grown on multi-electrode arrays, the cellular infection state and the associated cell response are assessable by impedance measurements. Unlike endpoint assays, the host cell response is followed continuously in real time, label-free and noninvasively. Here, a sensor platform comprising hardware, software and disposable electrode arrays is described suitable for fully automated cell-based neutralization assays tailored for high throughput screening campaigns. To develop cost-effective, disposable electrode arrays for impedance measurements, we screen printed film electrodes made from conducting polymers on the bottom of multi-well plates. The polymer electrodes were characterized for their host cell compatibility and readout performance in comparison to established gold-film electrodes. Hard- and software were tailored for robust and routine use in virological assays. Virus titration, virus neutralization as well as antiviral drug (Efavirenz) intervention studies were conducted using vesicular stomatitis virus (VSV) pseudotypes or the Env HIV-1 infectious molecular clones Ce1176 and X1632 as viral model systems. The assays showed very similar analytical performance in terms of titration curves and dose–response relationships for polymer electrodes compared to commercial gold-film electrode arrays and reporter-based endpoint assays. Considering their technical advantages over established assays, impedance readings based on low-cost polymer electrode arrays may become an attractive alternative to conventional assays using luminescent or colorimetric readouts.

1 | Introduction

Most people consider vaccinations as a breakthrough of modern medicine, as they protect against potentially life-threatening bacterial and viral diseases. As such they serve the same purpose as antibiotic or virostatic drugs. But before a vaccine or drug is approved for use in humans, it is first tested for its effectiveness to ensure reliable protection. *Cell-based neutralization assays* and *drug efficiency studies* play an important role for the development of new vaccine candidates and drugs as well as quality assurance of already approved vaccines/drugs [1]. Vaccine efficacy testing is typically performed in the laboratory on cultured host cells, whose response to viral infection is analyzed in the presence of neutralizing antibodies in the blood serum from a previously vaccinated person. Many of the applied viruses must be handled in biosafety level (BSL) 3 or 4 laboratories. The use of virus mimicking alternatives, especially replication-incompetent pseudoviruses, can reduce safety requirements. Such pseudoviruses emulate both, the virus-receptor binding and the cell entry mechanism, but are unable to replicate. Due to replication incompetence, they are safe to work with and can be handled under BSL-1 or BSL-2 [2]. For easier detection of infected cells, the viruses are typically engineered to carry a reporter gene, for example the gene encoding the *Green Fluorescent Protein* (GFP) or a luciferase [3–6]. Upon virus entry into the cells, reporter protein expression starts, confirmed by recording of a green cytoplasmic fluorescence of the cells. Reporter gene expression has been proven to be directly proportional to the number of virus-infected cells. If the vaccination was not efficient, the neutralizing antibody titers in the serum are not sufficient to prevent viral infection of the cells. If the vaccination was successful, neutralizing antibodies against the viruses are present in serum in sufficient amounts and virus encounter remains without consequences for the cells. Thus, suppression of viral infection by neutralizing antibodies serves as a proof of the efficacy of a vaccine.

Established readouts for such assays are often fluorescence/luminescence based [3–6], are hardly automated and require expensive reagents [7]. Moreover, they operate as endpoint assay, providing no time resolution of the cellular response [8, 9]. Reporter gene expression can usually be monitored only after assay times of 24–48 h [10]. The shortcomings of these readouts represent a limiting factor in vaccine development.

Few years ago, electric cell-substrate impedance sensing (ECIS) was recognized as a suitable noninvasive and label-free method for measuring the dielectric properties of adherent cells during virus encounter in real time, thus overcoming the assay limitations mentioned above. The principle of ECIS is based on monitoring the electrochemical impedance Z between two cell-covered thin-film electrodes – deposited on the bottom of a cell culture vessel – over a broad frequency range while exposing the cells to a weak sinusoidal AC voltage or current. By measuring the steady-state current or voltage drop resulting from the excitation, the impedance *Z* of the system is determined as a function of frequency [11]. The cell culture medium serves as electrolyte closing the electric circuit between the two cell-covered electrodes [12–14]. Due to the dielectric properties of the plasma membrane, the cell bodies on the electrodes act like small insulating particles, forcing the current to flow around

(< 10 kHz) or through (> 10 kHz) the cell bodies depending on the AC frequency [12]. The cells are not affected or harmed by the voltages and currents that are used since they are in the range of several millivolts and a few microamperes, respectively [11]. The technique provides the response of the cell as a whole since it integrates over the entire cell body and is therefore referred to as a (w)holistic integrating measurement principle [15]. Dependent on the AC frequency used for impedance readings, ECIS allows continuous electrical tracking of cell-surface interactions [16] as well as cell-cell interactions and alterations in the morphology of adherent cells [11, 17]. The sensitivity of this technique enables monitoring a variety of phenotypic assays with high temporal resolution, like monitoring of cell proliferation, cell spreading and cell detachment [14, 16] as well as cell migration and wound healing, cell motility, barrier function of cell layers or cell viability/cell death in general [11, 14, 17–22]. However, the technique is not sensitive to suspended cells without contact to the electrode surface.

Up to now, only few authors have reported impedimetric readouts in virological assays. Cho et al. used Vero cells as host cells which were exposed to a herpes simplex virus (HSV) 24 h after seeding on gold-film electrodes. Viral infection of the adherent cells led to a morphological change of the cells due to the virus-induced cytopathic effects (CPE), which were sensitively followed by time-resolved impedance measurements over 200 h. Increasing virus loads of MOI 0.0006, MOI 0.006 and MOI 0.06 (MOI = multiplicity of infection = ratio of number of viruses to number of host cells) induced a decrease of impedance eventually down to values of a cell-free electrode, with the onset of impedance decrease showing a clear concentration dependency [23]. Further work on flaviviruses, West Nile viruses and St. Louis encephalitis viruses not only demonstrated the impedimetric detection of CPE after infection, but also impedimetric monitoring of specific interventions by preincubation with neutralizing antibodies [24] or antiviral drugs like Cidofovir to antagonize alpha-herpes-viruses [25]. Mildner et al. [26] monitored the host cell response after viral infection and subsequent cell death via label-free and time-resolved impedance measurements based on gold-film electrodes. In virus titration assays, the author mixed suspended human embryonic kidney cells (HEK293T) with well-defined amounts of the vesicular stomatitis virus G (VSV-G), carrying the GFP reporter gene. This host cell-virus mixture was allowed to settle on gold-film electrodes and the electrode impedance during cell attachment and spreading was monitored as a function of time to reveal the virus-mediated CPE. $TCID_{50}$ (half-maximal tissue culture infectious dose) values deduced from integrated impedance time courses compared favorably well with $TCID_{50}$ values obtained from fluorescence readouts of GFP expression in the host cells 24 h after virus exposure.

Even though the suitability of impedance measurements to monitor virological assays has been demonstrated independently by several labs, the method has only found very limited use in systematic vaccine studies or as a quality control tool to date. The standard electrode material is gold, which is known for its excellent biocompatibility [27], its chemical and biological inertness and its compatibility with cell adhesion [11]. However, a major disadvantage of gold is its cost. Since testing vaccine candidates or their continuous quality control requires

a huge number of parallel tests, the material cost for gold becomes a limiting factor. A cost-effective alternative to using expensive metals as electrode material is the use of organic conducting polymers as they combine sufficiently high electrical conductivity with their compatibility to printing processes as established for mass production. Poly(3,4-ethylenedioxythiophene) (PEDOT) is possibly the most prominent example and its successful use as electrode material for ECIS measurements has been reported recently [28, 29]. However, conductive polymers are usually quite insoluble in any solvent and, thus, difficult to handle. By doping PEDOT with the negatively charged copolymer poly(styrene sulfonate) (PSS), a water-soluble polyelectrolyte, PEDOT gets dispersed in the aqueous reaction solution during polymerization, yielding PEDOT:PSS [30], which is outstanding among all conducting polymers with respect to material properties and its compatibility with process technology [31]. It shows a useful conductivity (10 S/cm) and properties of a supercapacitor as it forms a swollen hydrogel in aqueous solutions with a huge effective surface area. Moreover, PEDOT:PSS is stable in aqueous media (no adhesion loss), biocompatible and optically transparent when deposited as a thin film, allowing the inspection of cells grown on PEDOT:PSS electrodes using phase contrast microscopy.

Our concept is to provide a cost-effective impedance platform for fully automated, time-resolved and label-free monitoring of host cells during virus infection suitable for high throughput screening campaigns. We aimed to replace the commonly used gold electrodes by electrodes made from PEDOT:PSS screen printed as thin-film electrodes on the bottom of disposable multi-well plates. To provide a complete stand-alone platform, tailored readout electronics to measure impedance under cell culture conditions and corresponding software with integrated data analysis are the two additional pillars in addition to the PEDOT:PSS-based electrode arrays. In this study, we tested functional models of this novel impedance platform by conducting (i) virus titer quantification (titration assay) and (ii) quantification of neutralizing antibody responses (neutralization assay). Furthermore, results were validated using state-of-the art optical reporter gene-based endpoint assays and impedance measurements conducted with the established gold-film electrodes.

2 | Materials and Methods

2.1 | Cell Lines and Culture Conditions

All cell culture work was performed under a class II sterile bench (HERAsafe, Thermo Fisher Scientific Inc. USA). Non-sterile solutions as well as consumables were autoclaved for 20 min at 120°C (DX-45, Systec, Germany) before use. Solutions and media were pre-warmed to 37°C in a water bath (TW12, Julabo GmbH, Germany) before they got in contact with cells. The cells were routinely cultured at 37°C and 5% (v/v) CO_2 in a humidified incubator (Heraeus Function Line, Thermo Fisher Scientific Inc. USA). Cell culture media were changed every 2–3 days. Unless otherwise stated, all chemicals were purchased from Merck KGaA (Germany). The cell lines were subcultivated once a week (NRK cells) or every 3–4 days (HEK293T cells; TZM-bl cells) by means of standard trypsinization protocols

using buffered trypsin solutions containing 0.05% (w/v) trypsin and 1 mM EDTA in PBS^{--}. After cell detachment and centrifugation, the cell pellet was resuspended in culture medium and split in a ratio of 1:20 (NRK cells) or 1:10 (HEK293T cells; TZM-bl cells), respectively, based on the original cell density per cm² growth area. Suspended cells were counted using a Buerker hemacytometer (Marienfeld Superior, Germany) and diluted in culture medium to the appropriate seeding density before inoculation.

Normal Rat Kidney (NRK-52E; Leibniz Institute DSMZ GmbH, Germany) cells were cultured in Dulbecco's Modified Eagle's Medium (DMEM) containing 4.5 g/L D-glucose and 3.7 g/L $NaHCO_3$ supplemented with 5% (v/v) fetal bovine serum (FBS; Thermo Fisher Scientific), 2 mM L-glutamine, 100 U/ml penicillin and 100 µg/mL streptomycin.

Human embryonic kidney 293T (HEK293T; Leibniz Institute DSMZ GmbH, Germany) cells were cultured in DMEM containing 4.5 g/L D-glucose and 3.7 g/L $NaHCO_3$ supplemented with 10% (v/v) FBS (Thermo Fisher, Germany), 2 mM L-glutamine, 100 U/mL penicillin and 100 µg/mL streptomycin.

TZM-bl cells were obtained from the NIH AIDS Research and Reference Reagent Program (Cat. no. 8129), contributed by J.C. Kappes and X. Wu. The TZM-bl cell line is derived from a HeLa cell clone that was engineered to express CD4, CCR5 and CXCR4 [32] and to contain Tat-responsive reporter genes for firefly luciferase and _Escherichia coli_ β-galactosidase under control of an HIV-1 long terminal repeat [33]. The cells were cultured in DMEM containing 4.5 g/L D-glucose and 3.7 g/L $NaHCO_3$ (Fisher Scientific GmbH, Germany) supplemented with 10% (v/v) heat-inactivated FBS, 4 mM L-glutamine, 1 mM sodium pyruvate, 0.02 mM pyridoxine, 25 mM HEPES (4-(2-hydroxyethyl)-1-piperazineethanesulfonic acid) and 50 µg/mL gentamicin (Fisher Scientific GmbH, Germany).

2.2 | Fabrication of the Electrode Arrays Based on the Conducting Polymer PEDOT:PSS

Different multi-well formats of the disposable polymer electrode array have been developed and evaluated that differed with respect to electrode configuration, geometry and size. Figure 1A–C show electrode arrays in 8-well, 24-well and 96-well formats in their final layouts. All of them carry electrodes on the bottom of each well. The 8-well electrode arrays were only used in early phases of the project for rapid testing of different settings during screen printing. The fabrication steps were as follows. A transparent polyethylene terephthalate (PET) base plate (175 µm thickness) was functionalized by three different, screen printed layers: (i) The conductive polymer PEDOT:PSS (Heraeus Epurio GmbH, Leverkusen) as the active electrode material. We determined the average thickness of the PEDOT:PSS layer by analyzing cross-sections of the final electrodes using scanning electron microscopy. After complete curing, the conductive paste showed an average thickness of (440 ± 18) nm as determined from a total of twelve individual spots. Results are given as mean $\pm$ standard error. (ii) The conductive leads and contact pads for electrical connection to the hardware using nano silver screen printing paste with high conductivity (GenesInk, Rousset
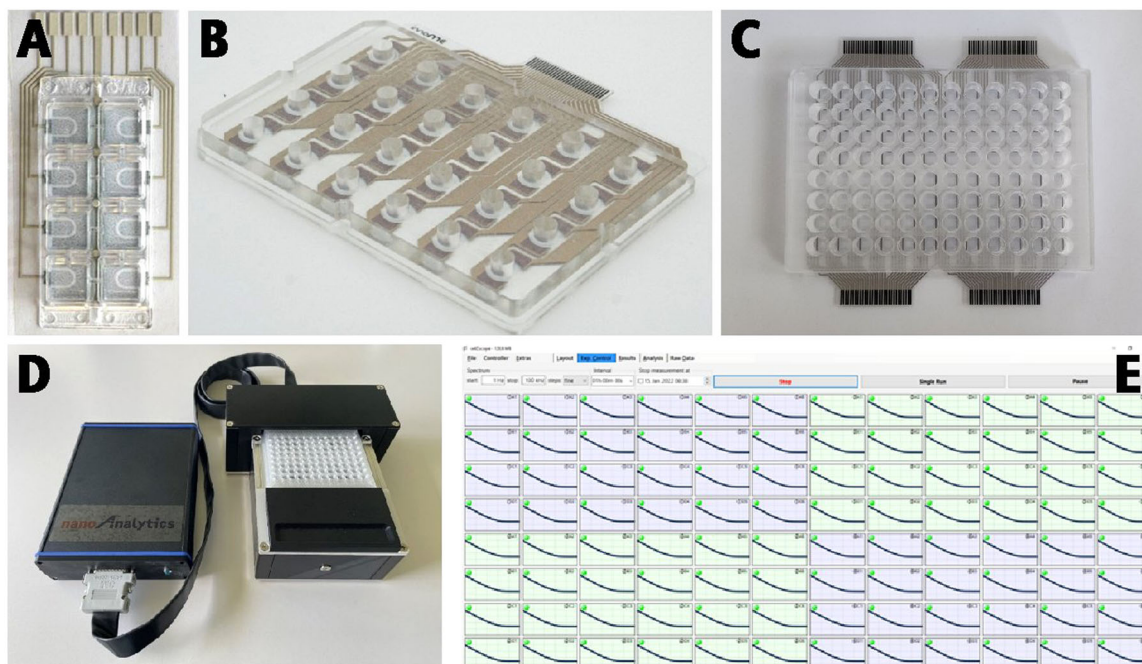
FIGURE 1 | (A–C) Functional models of the disposable PEDOT:PSS polymer electrode arrays in 8-well, 24-well and 96-well format. (D) Hardware to perform electrochemical impedance readings of adherent cells in individually addressable wells carrying the PEDOT:PSS electrodes. The electrode array is connected to the external cellZscope controller via a tailored array holder located inside a humidified incubator at 37°C and 5% CO_2 during the measurement. The controller is operated via the cellZscope software on a PC, providing data acquisition, visualization and processing (E).

Cedex, France). (iii) A biocompatible silicone passivation layer (DuPont de Nemours GmbH, Neu-Isenburg) of ~12 µm thickness, protecting the leads and defining the electrode layout – regarding size and shape – by openings in the passivation layer. The most sensitive electrode arrangement was a coplanar electrode configuration with four circular microelectrodes of same size (Ø$_{\text{screen printing mask}}$: 400 µm; Ø$_{\text{PEDOT:PSS electrode}}$: ~300 µm) located in the center of the well. Two of them were electrically connected to the other two by the bathing electrolyte but not by the PEDOT:PSS layer. So, two pairs of two circular microelectrodes each were measured against each other ("two vs. two"). Finally, a poly(methyl methacrylate) plastic body with individual openings defining the wells ($A_{\text{well}} = 0.34 \, \text{cm}^2$ for the 24-well and 96-well formats) was fixed to the PET base plate that carries the printed electrode layout using adhesive tape (3M Deutschland GmbH, Neuss), providing a mechanically stable and liquid-tight connection. A polystyrene lid added on top was used to reduce solvent evaporation and the risk of contamination. The PEDOT:PSS electrode arrays were stored under ambient conditions in the dark until being used for experiments. Before any cell-based assay, the electrode arrays were cleaned and sterilized by argon plasma treatment for 30 s (Plasma Cleaner PDC-002, Harrick plasma, USA). All measurements were performed in a humidified cell culture incubator at 37°C and 5% CO_2.

2.3 | Impedance Platform

To measure the impedance of the disposable electrode arrays under cell culture conditions, the hardware was tailored for robust and routine use in cell-based assays. For all impedance measurements, a modified cellZscope system from nanoAnalytics GmbH

(Muenster, Germany) was used. An array holder to connect the electrode arrays was placed inside a humidified incubator at 37°C and 5% CO_2. An external controller transmits the signals to a computer (Figure 1D) running a tailored version of the cellZscope software (nanoAnalytics GmbH) for data acquisition and analysis (Figure 1E), developed on the basis of the programming environment Visual Studio. The software allows flexible adjustment of all relevant experimental parameters (frequency range, number of repeated measurements, pauses, total duration of data recording), so that complete automation of the measurement is accessible including real-time visualization. It controls all hardware components of the experimental setup, stores data and enables subsequent offline data processing and analysis. Impedance spectra were recorded in a pre-defined frequency range between 1 Hz and 100 kHz, using a sinusoidal AC voltage of 50 mV (peak-to-peak). An AC voltage of 50 mV (peak to peak) used as amplitude for impedance measurements proved to be a useful compromise between non-invasiveness of the measurement, a sufficiently high signal-to-noise ratio and a linear current-voltage characteristic [34] required for data analysis. Depending on the frequency range, time resolution of the measurement was typically ~5 min in case of the 24-well format and ~20 min for the 96-well setup.

2.4 | Characterization of the PEDOT:PSS Polymer Electrodes

2.4.1 | Biocompatibility

Biocompatibility of the PEDOT:PSS electrode arrays was assessed by cell adhesion and cell growth studies. NRK cells were suspended in culture medium and seeded into the wells of

the electrode array (4.5×10^5 cells/cm^2). 24 h after seeding, the cell layer was live/dead stained using the Invitrogen LIVE/DEAD viability assay. The assay kit contains ethidium homodimer-1 (EthD-1; $\lambda_{exc} = 528$ nm, $\lambda_{em} = 617$ nm), providing a red nuclear fluorescence in dead or injured cells. The stock solution of EthD-1 in DMSO was diluted in PBS^{++} to a final concentration of $4\,\mu$M. The vital stain calcein acetoxymethylester (CAM; $\lambda_{exc} = 494$ nm, $\lambda_{em} = 517$ nm) is hydrolyzed to calcein in living cells providing a green cytoplasmic fluorescence. The stock solution of CAM in DMSO was diluted in PBS^{++} to a final concentration of $2\,\mu$M. To stain the cells 24 h after inoculation in the wells of the electrode array, the culture medium was removed, the cells were washed once with PBS^{++} and incubated with the freshly prepared EthD-1/CAM staining solution in the dark for 45 min at 37°C and 0% CO$_2$. After incubation, the cells were analyzed and imaged using an upright Nikon Eclipse 90i Confocal Laser Scanning Microscope in combination with a 10x objective (NA = 0.25).

2.4.2 | Performance in Electrochemical Impedance Analysis

The disposable polymer electrode array was characterized by impedance measurements and compared to established gold-film electrodes to unravel the specific electrochemical properties of the electrodes and to compare the performance in monitoring adherent cells. Before cell seeding, 200 μL/well of cell culture medium was added to each well and the baseline impedance of cell-free electrodes was recorded for 24 h at 37°C to allow for swelling and equilibration of the electrode material PEDOT:PSS (not necessary for gold-film electrodes). After stabilization of the electrode impedance, the cell culture medium in each well was replaced by 200 μL/well cell suspension (TZM-bl cells) at a seeding density of 2×10^5 cells/cm^2 and impedance measurements were continued for 24 h to follow cell attachment and spreading. To prove sufficient sensitivity of the electrode layout for virus neutralization assays, the CPE of lytic viruses was simulated using the plant detergent saponin as CPE surrogate. Saponins are a group of herbal glycosides with detergent properties and are known to cause cell lysis and cell death [35]. NRK cells were seeded to confluence on the electrode surface (4.5×10^5 cells/cm^2, 200 μL/well). 24 h after seeding, the cell culture medium was replaced by 100 μL/well Leibovitz's L-15 medium (Thermo Fisher Scientific, Germany) and the cells were allowed to equilibrate for 1–2 h (37°C, 0% CO$_2$). Thereafter, different concentrations of saponin diluted in L-15 medium were added as 2× working solutions to the cells (100 μL/well), giving final concentrations of 10, 15, 20, 25, 30, 50 and 75 μg/mL in the wells of the electrode array.

2.5 | Impedimetric Monitoring of Virus-Mediated Cell Infection

We compared the analytical performance of the PEDOT:PSS polymer electrodes with the established gold-film electrodes. In these benchmarking experiments, we used a commercial impedance platform (ECIS-Zθ, Applied BioPhysics Inc. Troy, NY) with 96-well gold-film electrode arrays (96W1E+) as a reference. Each well of the 96W1E+ electrode arrays contains two circular gold-film microelectrodes with 350 μm diameter. Three types of virological assays have been conducted, as these were the major motivation for the development of the polymer electrodes: (i) virus titer quantification (titration assay), (ii) quantification of neutralizing antibody responses (neutralization assay) and (iii) testing of drugs directed against viral infection. Impedance measurements were performed under standard cell culture conditions at 37°C and 5% CO$_2$ in a humidified incubator.

2.5.1 | Workflow of the Impedance-Based Virus Titration Assays

In virus titration assays, we monitored the time course of impedance during attachment and spreading of a constant number of host cells on PEDOT:PSS electrodes in comparison to gold-film electrodes as a function of virus load to follow virus-mediated cell infection.

Pseudoviruses derived from VSV were engineered to carry the GFP as reporter gene for independent optical control of host cell infection. They display the autologous *Glycoprotein* (VSV-ΔG*GFP + G) for host cell binding and membrane fusion on their surface and were used as lytic model virus to monitor virus-induced CPE. Pseudovirus design and recovery was supported by S. Einhauser and Prof. Dr. R. Wagner (Institute of Medical Microbiology and Hygiene, University of Regensburg). The virus titer was quantified by the *limited dilution focus forming assay*. Virus suspensions were stored at −80°C. HEK293T cells served as adherently growing host cells. To conduct the assay, PEDOT:PSS and gold-film electrode arrays were cleaned and sterilized by argon plasma treatment (30 s). Gold-film electrodes were coated with crosslinked gelatin to facilitate cell adhesion: (i) coating with 0.5% (w/v) gelatin in water for 2 h at room temperature (RT); (ii) gelatin crosslinking with 2.5% glutaraldehyde in water for 10 min; (iii) extensive washing (~ 10×) with water. PEDOT:PSS electrodes were left untreated to avoid the risk of possible incorporation of cytotoxic glutaraldehyde in the swollen PEDOT:PSS polymer during gelatin crosslinking. Before cell seeding, the baseline impedance of cell-free electrodes immersed in cell culture medium (200 μL/well) was recorded for at least 24 h to allow for swelling and equilibration of PEDOT:PSS. Impedance spectra were recorded in frequency ranges of either 1 Hz–100 kHz (PEDOT:PSS electrodes) or 62.5 Hz–64 kHz (gold-film electrodes) as two different impedance platforms had to be used for the individual electrode materials. HEK293T cells suspended in cell culture medium (10^6 cells/mL, 100 μL/well) were mixed with a well-defined suspension of the pseudoviruses (VSV-ΔG*GFP + G) at MOI (multiplicity of infection = ratio of number of viruses to number of host cells) 0.005–10. This host cell-virus mixture was seeded into the wells of the electrode arrays and the electrode impedance was monitored for 24 h during cell attachment and spreading in presence of the viruses as a function of time. For data analysis, the time courses of the normalized impedance (impedance normalized to values of cell-free electrodes in culture medium before cell seeding) at individual monitoring frequencies (gold: 40 kHz, PEDOT:PSS: 10 kHz) were integrated between 0 h (cell seeding) and 24 h using a constant baseline of

integration of $IZI_{norm} = 1$. The area-under-the-curve (AUC) was plotted versus the virus concentration (MOI) in a semi-logarithmic manner to extract a dose–response relationship. *Tissue culture infectious doses* with 50% efficiency ($TCID_{50}$) were calculated using a four-parameter logistic fit (OriginPro 2023) for the dose–response data.

The impedance readout was correlated with the expression of the virus-borne reporter gene in host cells after 24 h. GFP fluorescence intensity was recorded for each well of the electrode arrays using a TECAN GENios microplate reader (top read, λ_{exc}: 485 nm, λ_{em}: 535 nm, gain: 73). In addition, fluorescence micrographs of the cells were recorded at the Nikon Eclipse Ts2Fl inverse fluorescence microscope (λ_{exc}: 470 nm (LED), λ_{em}: 510 nm, 4× objective, 400 ms exposure time) for spatial control of reporter gene expression.

2.5.2 | Workflow of the Impedance-Based Virus Neutralization Assays

In impedance-based virus neutralization assays, we monitored the impedance time course of host cell adhesion on PEDOT:PSS electrodes alone or in comparison to gold-film electrodes. These assays were conducted in presence of a constant virus titer but increasing amounts of purified antibodies to test for their neutralizing capacity.

VSV-ΔG*GFP + G Pseudoviruses and α-VSV-G Neutralizing Antibody & HEK293T Host Cells: Neutralization of VSV-ΔG*GFP + G pseudoviruses was tested using the recombinant monoclonal antibody α-VSV-G (8G5F11, mouse, absolute antibody, Kerafast Inc. Shirley, MA). The antibody was stored in a concentration of 0.1 mg/mL in PBS^{++} at 4°C. Preparation of the electrode arrays and adjustment of HEK293T cell seeding density was as described before. The VSV-ΔG*GFP + G pseudoviruses were diluted in DMEM to a concentration of MOI 1 and mixed with well-defined concentrations of the α-VSV-G antibody (0.3 ng/mL–1 μg/mL). After incubation for 1 h at 37°C, the antibody-virus complexes were mixed with suspended HEK293T cells (10^6 cells/mL, 100 μL/well) and this mixture was seeded into the wells of the electrode arrays. Electrode impedance during cell attachment and spreading was monitored for 24 h as a function of time to reveal the neutralizing capacity of the antibodies. Impedance data were processed and further compared with respect to virus-borne GFP expression as described above. Inhibitory antibody concentrations with 50% efficiency (IC_{50}) were calculated using a four-parameter logistic fit (OriginPro 2023).

Env HIV-1 Clones Ce1176/X1632, Neutralizing Antibodies 2F5 and CH31 & TZM-bl Host Cells: Two Env HIV-1 infectious molecular clones, Ce1176_A3. LucR.T2A. ecto/293/17 (Ce1176) and X1632_S2_B10. LucR.T2A. ecto./293T/17 (X1632), were selected for HIV neutralization assays based on their suitability for impedance-based measurements. Further information on the established virus production is given in the Supporting Information S1: SI. Virus dilutions used in these neutralization assays have been determined in advance by virus titration assays (impedance and reporter gene based). For further information cf. II in SI. The broadly neutralizing antibodies (bnAB) 2F5 (Polymun Scientific Immunbiologische Forschung GmbH, Germany) and CH31, kindly provided by D.C. Montefiori (Duke University Medical Center, Durham, NC), were

used for virus neutralization. To conduct the impedance-based assays, PEDOT:PSS electrode arrays were prepared and equilibrated as described above. Threefold serial dilution (3×) of test reagents were prepared in cell culture medium, resulting in final assay concentrations of 0.02–50 μg/mL for either of the bnAB. Virus dilutions of 1:17 for Ce1176 and 1:13.5 for X1632 were added to each of the antibody preparations. The Env HIV-1 IMC/antibody mixtures (150 μL/well) were incubated for 60 min at 37°C and 5% CO_2. After incubation, TZM-bl cells (3×10^4 cells/well) suspended in cell culture medium containing 6 μg/mL DEAE-Dextran were added to each well of the electrode arrays. The electrode impedance was recorded for 70 h as a function of time. For data analysis, the time course of the normalized impedance recorded at a monitoring frequency of 3.6 kHz was integrated between 0 h (cell seeding) and 70 h using a constant baseline of integration of $IZI_{norm} = 1$. The AUC was plotted versus inhibitor concentrations on a semi-logarithmic scale to extract a dose–response relationship. IC_{50} values were calculated using a four-parameter logistic fit (OriginPro 2023). For an orthogonal readout, virus-induced expression of the *firefly luciferase* reporter gene in TZM-bl cells was tested by preparing threefold serial dilutions (3×) of the bnAB 2F5 and CH31 in a 96-well plate in cell culture medium, resulting in final assay concentrations of 0.01–25 μg/mL for each antibody. Env HIV-1 dilutions, adjusted to 1:225 to achieve a TCID of ~ 150.000 relative luminescence units (RLU), were added and incubated for 60 min (37°C, 5% CO_2). After incubation, TZM-bl cells (1×10^4 cells/well) suspended in cell culture medium containing 6 μg/mL DEAE-Dextran were added to each well to reach a final assay volume of 250 μL. Uninfected TZM-bl cells were used as background control and untreated infected TZM-bl cells as virus control. After incubation for 48 h (37°C and 5% CO_2), 150 μL of the supernatant was removed, 100 μL Britelite plus reagent (Perkin Elmer GmbH, Germany) was added to the cells in each well and incubated for 2 min at RT to allow cell lysis. 150 μL of the cell lysate was transferred to a black microtiter plate and the luminescence was measured using a Victor 3 Luminometer (Perkin Elmer GmbH, Germany). Luminescence intensity was plotted in RLU versus inhibitory antibody concentrations in a semi-logarithmic manner to extract a dose–response relationship. IC_{50} values were calculated using a four-parameter logistic fit (OriginPro 2023).

2.5.3 | Workflow of the Impedance-Based Testing of Antiviral Drugs

These assays were conducted with the Env HIV-1 clones Ce1176 and X1632 exposed to the non-nucleoside reverse transcriptase inhibitor (NNRTI) Efavirenz (EFV). The experimental workflow was identical to the neutralization assays described in the preceding paragraph for the broadly neutralizing antibodies 2F5 and CH31. The reverse transcriptase inhibitor EFV was tested in concentrations in a range of 0.014–30 ng/mL EFV.

3 | Results and Discussion

3.1 | Design of Electrodes, Biocompatibility and Electrochemical Characterization

Among all conducting polymers, PEDOT:PSS stands out as it is available as an aqueous dispersion, making manufacturing and

handling reasonably easy. It is readily printable in homogeneous layers of well-defined thickness using screen printing. PEDOT:PSS is known for its good electrochemical performance in impedance analysis and it is stable for experimental times commonly used in cell culture studies under cell culture conditions, that is, it does not peel off the substrate in aqueous environments. The polymer is transparent for visible light when deposited as a thin film, allowing the inspection of cells on the electrode surface using phase contrast microscopy. During the design and optimization process of the polymer electrode array, different concepts for electrode geometry and size were evaluated. In principal, the electrode layout for the purpose described here is restricted to coplanar arrangements of two electrodes. Different design concepts for the electrodes (Figure 2) were considered: (i) one small working electrode and a significantly bigger counter electrode (Figure 2A) or (ii) two (Figure 2B), (iii) four (Figure 2C) or (iv) six (Figure 2D) circular microelectrodes of the same size arranged as pairs of one (ii), two (iii) or three (iv) parallel electrodes on two separated patches of PEDOT:PSS, so that these pairs are formally used as *working* or *counter* electrodes even though they are indistinguishable. Each of the four different electrode layouts was tested for increasing electrode diameters (Ø = 300–800 μm) to identify the best analytical performance. Choosing small diameters runs the risk of insulating the electrodes by inward flow of the

passivation material during screen printing. Moreover, the number of cells that contributes to the signal gets increasingly low. If the diameters are chosen too big, the sensitivity of the electrodes for the presence of cells decreases [11].

Impedance measurements using different model cell lines finally led to the compromise of using a coplanar electrode layout with four circular microelectrodes per well (Ø$_{screen\ printing\ mask}$: 400 μm; Ø$_{PEDOT:PSS\ electrode}$: ~ 300 μm) used in pairs of two as *working* and *counter* electrode (Figure 2C). This final electrode layout is a trade-off between sensitivity of the measurement, integration across the number of cells on the electrode and limitations of the printing process. We have included typical impedance spectra of the various electrode layouts together with our performance criteria in the supporting information. Translation into 96-well format yielded electrode arrays as schematically drawn in Figure 2E.

After the multiple layers of (a) PEDOT:PSS as electrode material, (b) nano silver paste for the conductive leads plus contact pads and (c) silicone as the passivation layer defining electrode geometry and size had been screen printed upon the base plate, the final PEDOT:PSS electrodes on the bottom of each well were studied in detail. Phase contrast micrographs show a clearly delineated, circular opening in the passivation layer (Figure 3A)
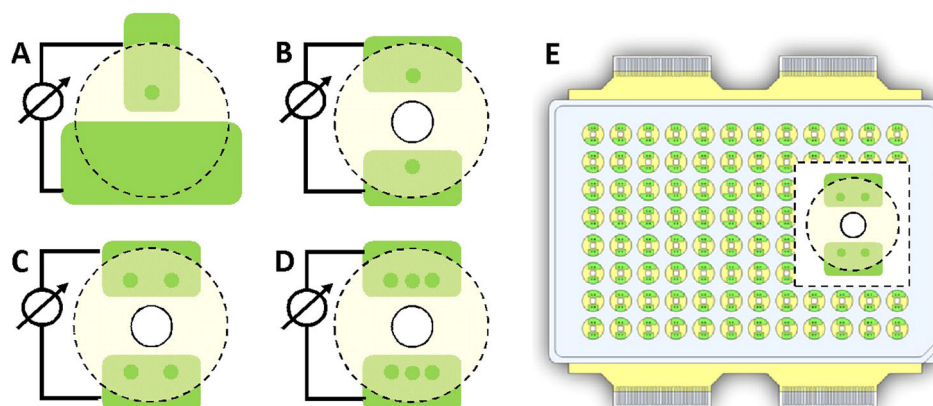

FIGURE 2 | Different electrode layouts were tested for their suitability for cell-based assays: white: base substrate; green: PEDOT:PSS; bright yellow: passivation; dashed line: well perimeter; white circle: optical window for high resolution microscopy. (A) Small (working) electrode in series to big (counter) electrode; (B) individual circular electrodes in series; (C) pairs of two circular electrodes in series; (D) pairs of three circular electrodes in series. (E) Final layout (C) translated into 96-well format.
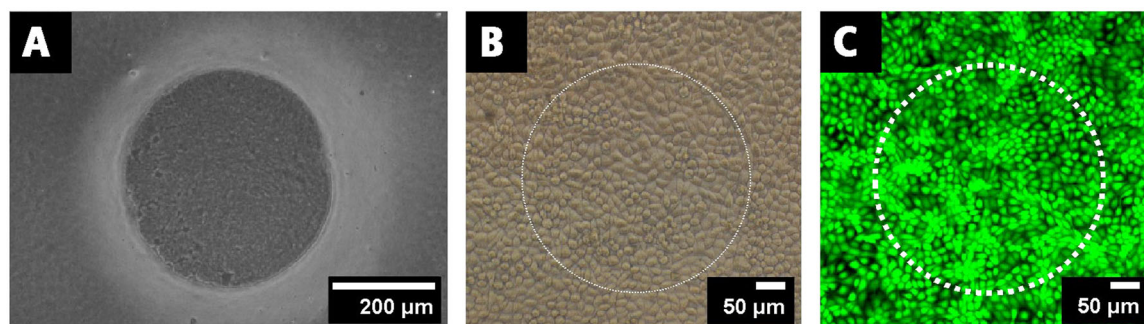

FIGURE 3 | (A) Phase contrast micrograph of one cell-free circular PEDOT:PSS polymer electrode, that is, the circular opening in the silicone insulation layer. Typical phase contrast micrograph (B) and fluorescence micrograph after vital stain (C) of TZM-bl cells grown to confluence on such printed PEDOT:PSS polymer electrodes. Images were recorded 24 h after cell seeding (2×10^5 cells/cm^2). The white circle in (B) and (C) delineates the electrode border.

defining the active electrode. Using a screen printing mask with an opening of 400 µm diameter for printing the insulation layer, yielded an average diameter of the circular shaped PEDOT:PSS electrodes of (298 ± 20) µm (n = 26). The reduced diameter of the final electrode relative to the diameter provided by the mask is mainly due to unintended inflow of the insulation paste into the opening. This reduction in electrode diameter is inherent to the printing process and requires corresponding compensation on the level of the mask.

An unconditional prerequisite for any electrode material to be used for cell-based assays is biocompatibility. PEDOT:PSS is clearly biocompatible as documented by microscopy for TZM-bl cells 24 h after seeding the cells to confluence on the electrode surface. Phase contrast micrographs (Figure 3B) show cells with their typical cobblestone morphology grown on the printed PEDOT:PSS electrode as well as on the silicone passivation layer demonstrating biocompatibility of both materials. The cells also bridge the step between passivation layer and PED-OT:PSS. Since the edge of the polymer electrode is poorly visible as soon as cells cover the surface, a white circle was added to the micrograph, delineating the electrode perimeter (Figure 3B). Figure 3C shows almost exclusively cells with a green cytoplasmic fluorescence and hardly any red emitting nuclei after a calcein AM/ethidium homodimer-1 (CAM/EthD-1) vital stain indicating the vast majority of cells are vital with an intact cell membrane. In CAM/EthD-1 stains, living cells with active enzymes convert nonfluorescent calcein AM to calcein which emits a green fluorescence and labels living cells accordingly. Ethidium homodimer-1 only emits fluorescence after it has intercalated into the DNA. But since EthD-1 is not membrane permeable, its red emission is only visible when the plasma membrane is compromised and the cell is lysed. Taken together, there have been no microscopic observations that would question the biocompatibility of the selected materials.

The PEDOT:PSS electrodes were further characterized by impedance analysis and compared to established gold-film electrodes as the state-of-the-art electrode material for monitoring cell-based assays. Figure 4A compares impedance spectra of cell-free electrodes (only covered with cell culture medium) and cell-covered (TZM-bl cells) electrodes of similar diameter and layout (small working electrode vs. big counter electrode) prepared from either PEDOT:PSS ($\varnothing_{electrode} = 280$ µm) or gold ($\varnothing_{electrode} = 250$ µm). Impedance data was recorded over a broad frequency range from 1 Hz to 100 kHz applying 50 mV excitation amplitude. The impedance spectra of the cell-free electrodes differ in two main aspects: (i) The frequency-independent region towards the high frequency end of the spectra, where impedance is dominated by the constriction resistance of the microelectrodes, the ohmic resistance of the bulk electrolyte and the resistance of the leads, stretches over almost three decades from 200 Hz to 100 kHz for PEDOT:PSS but hardly converges to constant impedance values above 50 kHz for gold electrodes. In this regime, the impedance is lower for gold-film electrodes (1000 Ω) than for PEDOT:PSS electrodes (3000 Ω). The reason for this difference in high frequency impedance is the higher sheet resistance of PEDOT:PSS film electrodes compared to gold. Based on the data sheet provided by the manufacturer, the PEDOT:PSS film has a sheet resistance of 700 Ω/square (film thickness app. 200 nm) whereas gold is reported to have a sheet resistance of less than 1 Ω/square (film thickness app. 50 nm) [36]. As the high frequency impedance of the electrodes masks the impedance of the cells in series to the electrode, sensitivity decreases with increasing high frequency impedance of the electrodes [11]. This observation is in favor of gold as electrode material.

(ii) The close-to-linear decrease of the impedance at low frequencies – dominated by the interface impedance between electrode and electrolyte – shows a parallel shift towards significantly lower frequencies for PEDOT:PSS compared to gold-film electrodes. This phenomenon is assigned to the higher interface capacitance of PEDOT:PSS film electrodes due to their hydrogel like structure providing an enormously high interfacial area and charge transfer from the electrolyte into the hydrogel. Gold-film electrodes are rather flat and almost ideally polarizable. They do not allow for such a charge transfer across the electrode/electrolyte interface as long as there are no redox-active molecules in the medium. Typically, there are none. For a more quantitative comparison, we calculated the interface capacitance for frequencies in the linear regime towards the low
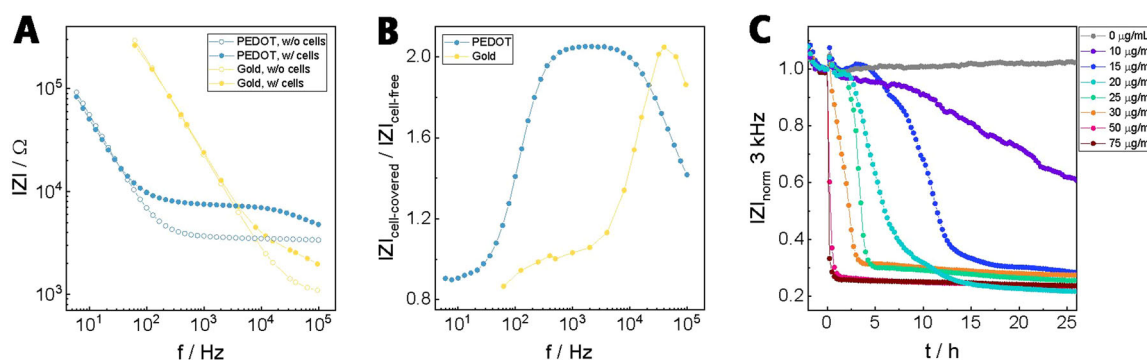

FIGURE 4 | Impedance spectra (A) for cell-free and cell-covered (confluent TZM-bl cell layer) electrodes of similar size (PEDOT:PSS: $\varnothing_{electrode} = 280$ µm, gold: $\varnothing_{electrode} = 250$ µm) and layout (working electrode vs. counter electrode). (B) To present the normalized impedance spectra for both electrode materials, the impedance of the cell-covered electrode (A) was divided by the impedance of the cell-free electrode (A) for every frequency. (C) Time course of the normalized impedance $|Z|_{norm}$ at 3 kHz for the PEDOT:PSS electrodes during exposure of NRK cells to saponin in different concentrations in L-15 medium. Saponin was added at time zero. NRK cells were seeded to confluence on the electrodes 24 h before saponin addition.

frequency end of the spectrum. The calculation returned a capacitance of $14\,\mu F/cm^2$ for gold (at $1\,kHz$) compared to $432\,\mu F/cm^2$ for the PEDOT:PSS electrodes (at $10\,Hz$). This shift of the interface impedance to lower frequencies increases the sensitivity of PEDOT:PSS electrodes for the presence of cells, as the difference between electrode capacitance and cell layer capacitance gets significantly bigger, providing a much bigger frequency window for sensitive recordings of cell-based assays. This fact is in favor of PEDOT:PSS as electrode material and the most prominent difference to classical noble metal electrodes.

The presence of a confluent cell layer on the PEDOT:PSS electrodes leads to an increase of the impedance, clearly visible in the frequency range between $100\,Hz$ to $20\,kHz$ by the formation of a plateau that delineates the frequency region that is suitable for sensitive impedance measurements monitoring cell-based assays. The presence of cells on PEDOT:PSS electrodes dominates the impedance spectrum over a broad frequency range, whereas on gold electrodes, this frequency range is significantly narrower. This is also expressed in the normalized impedance spectra, obtained by dividing the impedance of cell-covered electrodes by the impedance of cell-free electrodes for every discrete frequency giving bell-shaped curves (Figure 4B). The AUC is a quantitative measure for the *integral sensitivity* of the electrodes under test. Integration between $100\,Hz$ and $100\,kHz$ returns an AUC (ignoring units) of 1.01 for gold and 2.63 for PEDOT:PSS. Accordingly, PEDOT:PSS electrodes show a higher sensitivity along the full frequency spectrum and are superior to gold, particularly in the low frequency range of the spectrum that is dominated by impedance contributions of cell-cell and cell-substrate contacts. The *differential sensitivity*, which refers to the maximum impedance contribution of the cells to the total impedance of the system at one discrete frequency, corresponds to the maximum of the normalized impedance (peak value). It is very similar for both electrode materials and amounts to approximately two for these cells. In all practical terms, impedance measurements provide similar sensitivities for both electrode types at the peak frequency.

An important criterion for the suitability of the electrode array for virological assays is a sufficiently high sensitivity for cytopathic changes in cell morphology upon viral infection of cells. To simulate infection of cells by a lytic virus, that permeabilizes the plasma membrane, a confluent NRK cell monolayer grown on PEDOT:PSS electrodes was exposed to the plant detergent saponin which is known to induce membrane permeabilization and finally cell death. The cell response was followed by single frequency impedance measurements at $3\,kHz$ which corresponds to the peak of the normalized impedance for PEDOT:PSS electrodes to provide maximum sensitivity. If distinction between trans- or paracellular current pathways is of prime interest and sensitivity is not the most important criterion for the experiment, a higher or lower monitoring frequency – even aside from the plateau region – might be meaningful. However, such a pathway analysis was not in the scope of this study. Figure 4C shows the time courses of the normalized impedance IZI_{norm} (normalized to the last impedance value before saponin addition) for confluent NRK cell layers exposed to different concentrations of saponin $24\,h$ after seeding to confluence. Addition of $75\,\mu g/mL$ and $50\,\mu g/mL$ saponin induces an instant drop of IZI_{norm} down to the value of a cell-free electrode indicating instantaneous cell lysis. For lower concentrations, the impedance drop is delayed depending on the saponin concentration. The higher the concentration, the faster and more abrupt is the impedance decline. The latter mirrors the concentration dependent time courses of cell membrane permeabilization. These experiments reveal that the cellular response to lytic stimuli is readily detected as a function of stimulus concentration, proving the sensitivity of this platform to monitor the CPE after lytic virus exposure.

3.2 | Monitoring Virus Titration Assays by Impedance Measurements With Screen Printed Polymer Electrodes

The performance of the PEDOT:PSS electrode arrays in 96-well format was compared to established gold-film electrodes in a set of virological assays. For the first benchmarking experiment, a virus titration assay was conducted. In virus titration assays, cells are exposed to different virus concentrations. The *tissue culture infectious doses* ($TCID_{50}$) are determined from the cell response upon infection. This provides information on the viral dose required to infect 50% of the cell population or to trigger a CPE in 50% of the cells.

In this impedimetric virus titration assay, we monitored the impedance time course of host cell attachment on PEDOT:PSS in comparison to gold-film electrodes in presence of increasing virus loads. The pseudovirus VSV-ΔG*GFP + G, carrying a GFP reporter gene that is expressed in the host cells upon infection, was used as lytic model virus in combination with HEK293T host cells. Cell entry of the virus occurs via attachment of the glycoprotein G to the low density lipoprotein receptors (LDL-R) on the host cell surface and subsequent fusion with the cell membrane [37]. Upon host cell entry, viral replication processes start and finally, CPEs lead to cell death [38, 39]. The suspended host cells were mixed with a well-defined suspension of the pseudoviruses at MOI 0.005–10, followed by seeding into the wells of the electrode arrays (time zero). The time courses of the normalized impedance (normalized to IZI values of cell-free electrodes in culture medium before cell seeding) were recorded at the individual, most sensitive recording frequency (PEDOT:PSS: $10\,kHz$, gold: $40\,kHz$).

Figure 5 shows a comparison of the time courses of the normalized impedance for the PEDOT:PSS electrode array (**A**) and the commercial gold-film electrode array (**B**) after cell seeding at time zero. Under control conditions without any viruses, IZI_{norm} increases instantaneously due to cell attachment, passes through a maximum after $2.5\,h$ and increases again, but less steeply, until the end of the measurement. This second continuous increase in IZI_{norm} indicates the continuation of cell spreading and the onset of cell proliferation. The decrease in IZI_{norm} after passing the transient maximum at $2.5\,h$ is most likely due to morphological rearrangements of the cells on the electrode surface. Host cell attachment in presence of the viruses shows a clear concentration dependency in the impedimetric profile (Figures 5A1, 5B1). For low virus concentrations (MOI 0.005–0.1), the impedance time courses are very similar to the time courses of the medium control, indicating that the cells remain unaffected. IZI_{norm} reaches somewhat

lower values with increasing MOI values towards the end of the observation time (more pronounced for gold), already indicating virus-mediated cell lysis in case of MOI 0.1. Medium virus concentrations for MOI 0.5 and 1 show only the first transient impedance increase and lack the second one. For MOI 2, 5, 7 and 10, the initial increase in IZI_{norm} is followed by a monotonous decrease to values of a cell-free electrode. This indicates increasingly severe CPEs [40] visible already after 5 h. Micrographs in Figure 6 prove that the infected host cells, expressing the virus-borne GFP reporter protein, remain attached to the surface even for high virus loads. Thus, we conclude that infected cells shrink due to the onset of apoptosis or a related form of cell death and thereby open up new current pathways reducing the electrode impedance. $TCID_{50}$ values were determined by integration of the normalized impedance time courses (AUC, 0–24 h) and logistic fitting of the concentration-dependent AUCs, resulting in values of MOI (0.57 ± 0.07) for

the PEDOT:PSS electrode array and MOI (0.9 ± 0.2) for commercial gold-film electrode arrays (Figure 5A2, 5B2). These $TCID_{50}$ values compare very favorably indicating a similar performance of both electrode materials. Quantitative support for this conclusion is provided by Spearman correlation analysis which assesses how well the relationship between two variables – independent of their normal distribution – is described by a monotonic function. Perfect correlation provides a Spearman correlation coefficient of 1. For the correlation between impedance readings using PEDOT:PSS electrodes on the one hand and gold-film electrodes on the other, calculation returned a Spearman coefficient of 0.879 ($p < 0.001$). The more often used Pearson correlation coefficient is used to describe a potential linear correlation. The calculation returned 0.968 ($p < 0.001$). Accordingly, monitoring the host cells by fully automated impedance readings using PEDOT:PSS or gold-film electrodes provides highly correlated results and the same $TCID_{50}$ within error limits.
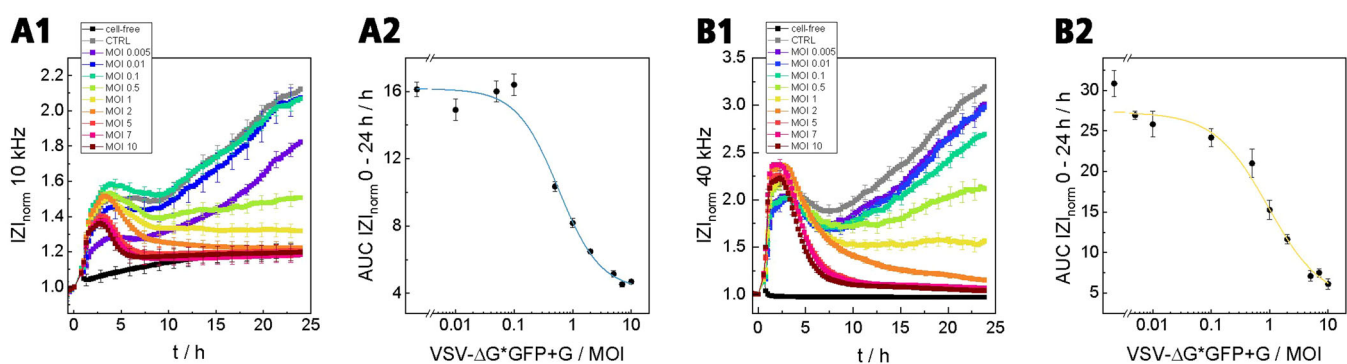

FIGURE 5 | Impedance-based virus titration assay. Time course of the normalized impedance IZI_{norm} at 10 kHz (PEDOT:PSS) and 40 kHz (gold), respectively, during HEK293T cell attachment on PEDOT:PPS electrodes (A1) and commercial gold-film electrodes (B1) in presence of different VSV-$\Delta G^*GFP + G$ pseudovirus concentrations (MOI 0.005–10). HEK293T cells suspended in cell culture medium were seeded (10^5 cells/well) into the wells of the electrode array in presence of the viruses at time zero. (A2, B2) Area under the curve for IZI_{norm} between 0 and 24 h plotted against the virus concentration (MOI) to determine the $TCID_{50}$ for cells grown on PEDOT:PSS (A2) and gold-film electrodes (B2). Values for the lowest virus load correspond to a virus-free control. $TCID_{50}$ values were calculated to be MOI 0.57 ± 0.07 for PEDOT:PSS electrodes and MOI 0.9 ± 0.2 for gold-film electrodes using a four-parameter logistic fit (OriginPro 2023). $n \geq 4$, mean $\pm$ SEM.
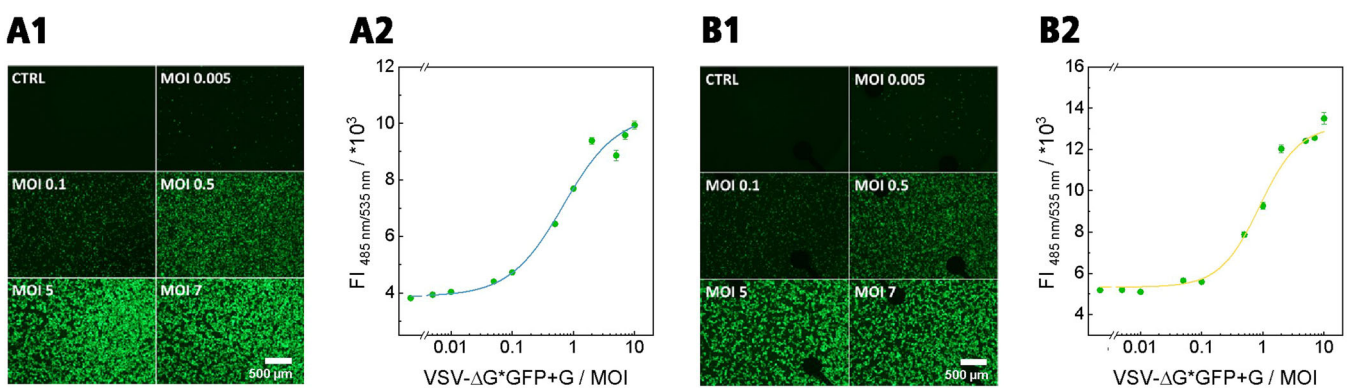

FIGURE 6 | Virus titration assay. Fluorescence micrographs of HEK293T cells 24 h after VSV-$\Delta G^*GFP + G$ pseudovirus exposure in different concentrations (MOI) to quantify reporter gene (GFP) expression on PEDOT:PSS electrodes (A1) and commercial gold-film electrodes (B1), respectively. HEK293T cells suspended in cell culture medium were seeded (10^5 cells/well) into the wells of the electrode array in presence of the viruses at time zero. The dark structures in B1 correspond to the gold-film electrodes on the bottom of the well. (A2, B2) GFP fluorescence intensity (FI) in each well of the electrode array recorded with a microplate reader 24 h after virus exposure and plotted against the virus concentration (MOI) to determine the $TCID_{50}$ for cells grown on PEDOT:PSS (A2) and gold-film electrodes (B2). Values for the lowest virus load correspond to a virus-free control. $TCID_{50}$ values were calculated to be MOI 0.7 ± 0.1 for PEDOT:PSS electrodes and MOI 0.9 ± 0.2 for gold-film electrodes applying a four-parameter logistic fit (OriginPro 2023). $n = 8$, mean $\pm$ SEM.

Virus infection of the cells was also evaluated based on virus-mediated reporter gene expression 24 h after virus exposure by reading the integral GFP fluorescence intensity using a microplate reader as well as by recording fluorescence micrographs (Figure 6). The fluorescence micrographs (Figure 6A1, 6B1) show an increasing cytoplasmic fluorescence of the cells with increasing MOI for both electrode materials, PEDOT:PSS and gold. Logistic fitting of the integral fluorescence intensities recorded by a microplate reader and plotted versus the virus concentration yields $TCID_{50}$ values of MOI (0.7 ± 0.1) for PEDOT:PSS electrodes and MOI (0.9 ± 0.2) for gold-film electrodes. The results are not significantly different. We conclude from this data that virus infection of host cells grown on screen printed PEDOT:PSS electrodes is quantitatively assessable by means of impedance measurements, resulting in $TCID_{50}$ that are not significantly different from luminescence readouts of well-established reporter gene assays with similar sensitivity as provided by commercial gold-film electrodes.

A Spearman correlation analysis between impedance-based assays and analysis of the virus-borne GFP expression has been demonstrated in a more recent study [41]. It returned a clear correlation between impedance analysis and reporter gene expression (Spearman coefficient of 0.873 ($p < 0.001$)). The paper also discusses other *key performance indicators* of both readouts, like sensitivity, time resolution, assay time, scalability and suitability for high throughput applications (Z' factor).

3.3 | Monitoring Virus Neutralization Assays by Impedance Measurements With Screen Printed Polymer Electrodes

In the second set of experiments, the virus neutralization assay, we monitored the host cell (HEK293T) response to virus (VSV-ΔG*GFP + G) exposure in presence of different amounts of purified neutralizing antibodies (α-VSV-G). In virus neutralization assays, the average inhibitory concentration (IC_{50}) of the antibody is determined at which half-maximal inhibition of viral infection occurs. To determine the IC_{50} of neutralizing antibodies, a constant concentration of the pseudovirus VSV-ΔG*GFP + G (MOI 1) was mixed with different amounts of the VSV-G specific monoclonal antibody α-VSV-G (0.3 ng/mL–1 μg/mL). These antibody-virus complexes were first incubated alone for 1 h and then mixed with suspended HEK293T cells, followed by seeding into the wells of the electrode array. Again, the time course of the normalized impedance IZI_{norm} was used to mirror host cell attachment in presence of the antibody-virus mixtures for 24 h to assess the neutralizing capacity of the antibody. Again, the performance of PEDOT:PSS electrodes was compared to gold-film electrodes as internal reference.

Figure 7 summarizes the results of this study for PEDOT:PSS electrode arrays (**A**) and for commercial gold-film electrode arrays (**B**). Impedance time profiles for both electrode materials (seeding at time zero) are rather similar. Host cell attachment mirrored in the impedance profiles is clearly dependent on the concentration of the neutralizing antibody with constant virus

load. The time courses of IZI_{norm} for antibody concentrations higher than 10 ng/mL are similar to IZI_{norm} for control conditions (cell seeding in medium only, Figure 5), revealing the typical adhesion characteristics of HEK293T cells. After cell seeding, IZI_{norm} instantaneously increases due to cell attachment and spreading upon the electrode surface, passes through a maximum after 2.5 h and then increases again, but less steeply, until the end of the measurement, indicating further cell spreading and proliferation. Thus, antibody concentrations higher than 10 ng/mL completely block viral infections; the cells remain unaffected and vital, proceeding with their attachment on the electrodes similar to the medium control. An antibody concentration of 10 ng/mL of α-VSV-G causes a half-maximal change in the impedance signal after 24 h, indicating partial neutralization of the pseudoviruses' impact on the host cells. For lower antibody concentrations of 3, 1 and 0.3 ng/mL, host cell attachment in presence of the antibody-virus mixture induces a transient increase followed by an impedance decrease to stable values within 10 h after seeding the cell-antibody-virus mixture on the electrodes, similar to the virus-only control. These impedance profiles indicate that virus neutralization was not complete and the host cells got infected, showing signs of CPE similar to virus exposure at MOI 1 in absence of neutralizing antibodies. Logistic fitting of the integrated normalized impedance time courses over 24 h yields similar inhibitory antibody concentrations with IC_{50} values of (10 ± 2) ng/mL for the PEDOT:PSS electrode array and (11 ± 3) ng/mL for commercial gold-film electrodes.

Fluorescence micrographs as well as integrated GFP fluorescence intensity readings 24 h after seeding the cells in presence of the antibody-virus mixture document virus-borne GFP reporter gene expression only in those cells that were infected by the virus (Figure 7A3, 7B3), confirming the results from impedance analysis. Logistic fitting of the fluorescence intensities integrated across the entire well and plotted versus the antibody concentration returns IC_{50} values of (10 ± 1) ng/mL α-VSV-G for PEDOT:PSS electrodes and (6 ± 1) ng/mL α-VSV-G for gold-film electrodes. Please note: To determine the IC_{50} and its error for PEDOT:PSS electrodes, we had to set and fix the slope of the logistic function to a typical value of 3 as the fit did otherwise not converge due to data structure. A slope of 3 was a typical value we found in this kind of dose–response relationship and it provided a better chi² of the best parameter fit than any other slope we tested. Table 1 summarizes the results from virus titration and virus neutralization assays performed with PEDOT:PSS electrodes in comparison to the established gold-film electrodes.

From the benchmarking experiments described in the preceding paragraphs, two conclusions apply: (i) Impedance-based analysis of virus titration and virus neutralization assays show very similar analytical performance independent of the electrode material: screen printed PEDOT:PSS versus thin gold-films. (ii) Moreover, the impedance readout corresponds favorably to state-of-the-art quantification of virus-induced reporter gene expression. Taken together, electrodes made from cost-efficient, screen printed PEDOT:PSS electrodes provide a reliable basis for noninvasive impedimetric monitoring of cell-based assays in general and virological assays in particular.
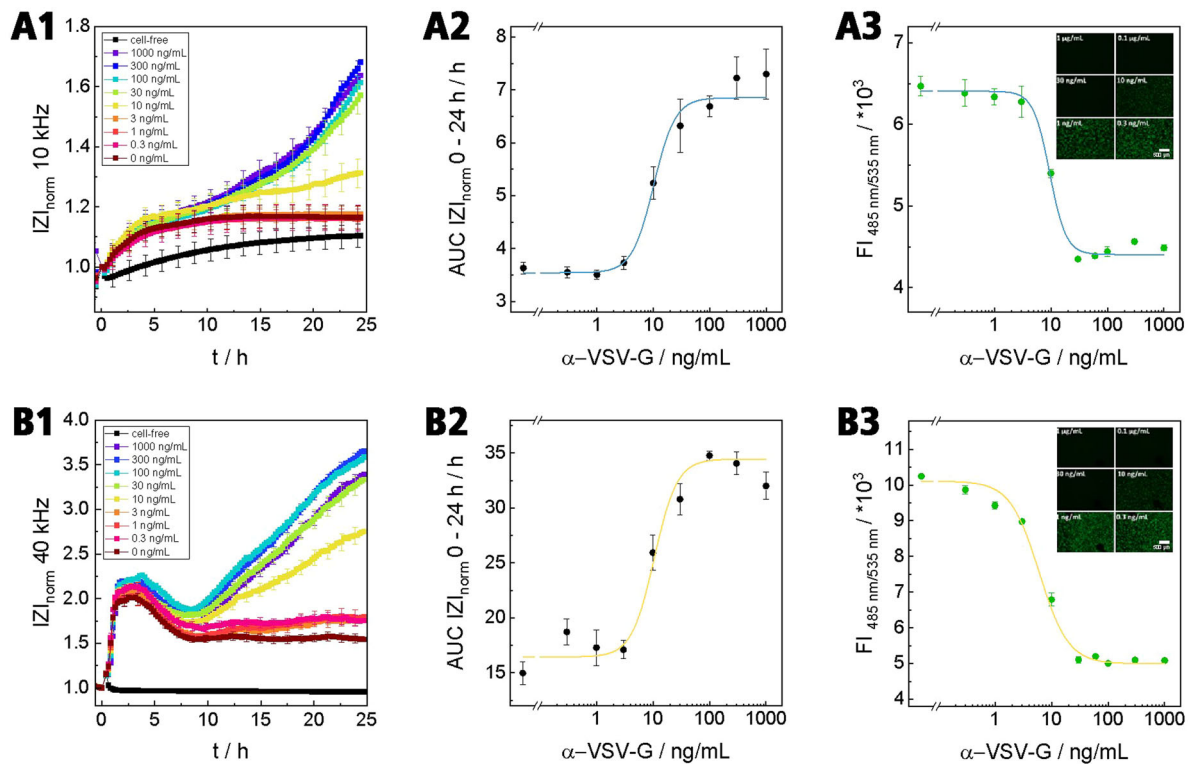
FIGURE 7 | Virus neutralization assay. Time course of the normalized impedance IZI_{norm} during HEK293T cell attachment on PEDOT:PPS (10 kHz) electrodes (A1) and commercial gold-film (40 kHz) electrodes (B1) in presence of the pseudovirus VSV-ΔG*GFP + G at MOI 1 and different amounts of α-VSV-G neutralizing antibodies (0.3 ng/mL–1 μg/mL). HEK293T cells suspended in cell culture medium were seeded (10^5 cells/well) into the wells of the electrode array in presence of the antibody-virus complexes at time zero. (A2, B2) Area under the curve for IZI_{norm} between 0 and 24 h plotted against the neutralizing antibody concentration (ng/mL) to determine the IC_{50} for cells grown on PEDOT:PSS (A2) and gold-film electrodes (B2). Values for the lowest antibody concentration correspond to an antibody-free control. IC_{50} values were calculated to be (10 ± 2) ng/mL for PEDOT:PSS electrodes and (11 ± 3) ng/mL for gold-film electrodes using a four-parameter logistic fit (OriginPro 2023). $n \geq 5$, mean $\pm$ SEM. (A3, B3) Integrated GFP fluorescence intensity (FI) in each well of the electrode array recorded 24 h after antibody-virus exposure and plotted against the neutralizing antibody concentration (ng/mL) to determine the IC_{50} for cells grown on PEDOT:PSS (A3) and gold-film electrodes (B3). Values for the lowest antibody concentration correspond to an antibody-free control. IC_{50} values were estimated to be (10 ± 1) ng/mL for PEDOT:PSS electrodes and (6 ± 1) ng/mL for gold-film electrodes. $n = 8$, mean $\pm$ SEM. The inserts show fluorescence micrographs of HEK293T cells 24 h after VSV-ΔG*GFP + G pseudovirus exposure at MOI 1 in presence of different amounts of α-VSV-G neutralizing antibodies as microscopic control of reporter gene (GFP) expression.

TABLE 1 | Comparison of results returned from impedance or reporter gene readouts of virus titration and virus neutralization assays for screen printed PEDOT:PSS electrodes and gold-film electrodes as a reference. $TCID_{50}$ values (virus titration) and IC_{50} values (virus neutralization) are given as mean $\pm$ SEM (impedance: $n \geq 4$, reporter gene expression: $n = 8$).

Readout	Virus Titration $TCID_{50}$ in MOI	Virus Neutralization IC_{50} in ng/mL
Impedance/gold	0.9 ± 0.2	11 ± 3
Reporter gene/gold	0.9 ± 0.2	6 ± 1
Impedance/PEDOT:PSS	0.57 ± 0.07	10 ± 2
Reporter gene/PEDOT:PSS	0.7 ± 0.1	10 ± 1

3.4 | Virus Inhibition Assays Directed Against HIV Infectious Molecular Clones Monitored by Impedance Measurements With Screen Printed Polymer Electrodes

In the preceding paragraphs, the suitability of screen printed electrodes to be used in impedance-based monitoring of virus titration and virus neutralization assays has been demonstrated on the example of VSV pseudoviruses. This virus-host combination is a very valuable research tool, emulating the fundamental processes of virus infection and neutralization, but it does not have any clinical relevance. To test the performance of PEDOT:PSS electrodes on a more relevant viral species, we performed additional experiments using infectious molecular clones (IMC) of the human immunodeficiency virus (HIV) in combination with TZM-bl host cells. The latter have been derived from a HeLa cell clone engineered to express, among other heterologous proteins, a Tat-responsive reporter gene for

firefly luciferase under control of an HIV-1 long terminal repeat [33], providing sensitive measurements of infection from bioluminescence [42] as a reference to impedance-based readouts. With this system we conducted (i) virus neutralization assays, which are of significant clinical relevance during vaccine development, and tested (ii) the impact of antiviral drugs on HIV infections in this model system.

To investigate whether impedance readouts using PEDOT:PSS electrodes are competitive to established luminescence assays when it comes to detect neutralization of HIV-1 infectivity, TZM-bl cells were exposed to two different Env HIV-1 infectious molecular clones (IMC), namely Ce1176 and X1632. The latter were incubated with dilutions of the broadly neutralizing antibodies (bnAB) 2F5 and CH31, respectively. This virus-antibody mixture was finally combined with suspended TZM-bl cells and seeded into the wells of the electrode arrays. Impedance was monitored continuously for 70 h after start of exposure while luminescence, as an indicator for reporter gene expression, was recorded from the TZM-bl cell lysates as endpoint readout 48 h after start of exposure. Figure 8A,C summarize the experiments by means of dose–response relationships that compare impedance analysis of the host cell response (left axis) to measuring bioluminescence of the luciferase reporter gene (right axis). In either case, the IC_{50} values for both assays were quantified by fitting a four-parameter logistic function to the data. Results are summarized in Table 2.

Using IMC Ce1176, the impedance assay returned an IC_{50} of (2.2 ± 0.5) µg/mL, that is, the bnAB CH31 antibody concentration required for half-maximal neutralization. For comparison, in the luciferase assays we determined an IC_{50} of (3.7 ± 0.4) µg/mL under the same experimental conditions (Figure 8A). Even though these IC_{50} values are significantly different from a statistical view point (t-test, $p = 0.95$), they are very similar by all practical means. When the second IMC, namely X1632, was tested for neutralization by bnAB 2F5 (Figure 8C), the two orthogonal readouts returned IC_{50} values of (9 ± 4) µg/mL using impedance or (4.4 ± 0.7) µg/mL using bioluminescence. These two values are not significantly different from each other (t-test, $p = 0.95$), supporting our conclusion that impedance-based monitoring with screen printed PEDOT:PSS electrodes is similarly sensitive to monitor virus neutralization assays compared to the established bioluminescence readout. It is noteworthy, that impedance-based monitoring of these assays gives access to dose–response correlations for any exposure time, as data acquisition is continuous and in real time.

Similar experiments were conducted to test the non-nucleoside reverse transcriptase inhibitor (NNRTI) Efavirenz (EFV) for its efficiency to reduce or inhibit viral infection using again TZM-bl host cells exposed to the two infectious molecular clones Ce1176 and X1632. Figure 8B,D summarize the dose–response analysis that was established from recording impedance for 70 h (AUC) and endpoint analysis of bioluminescence after 48 h of
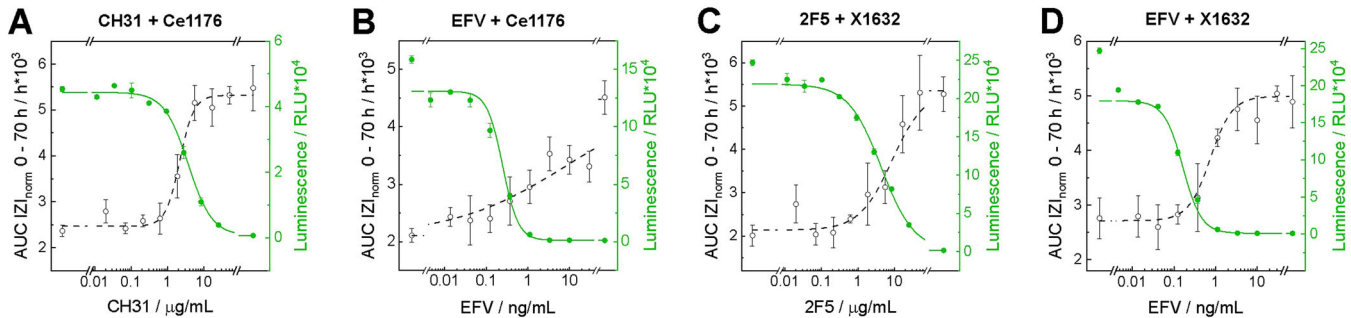

FIGURE 8 | Dose-dependent inhibitory response of TZM-bl host cells exposed to different amounts of bnAB CH31 (A) and NNRTI EFV (B) against Env HIV-1 IMC Ce1176 (A, B) and bnAB 2F5 (C) and NNRTI EFV (D) against Env HIV-1 IMC X1632 (C, D). Env HIV-1 IMC were preincubated with serial dilutions of bnAB or NNRTI EFV. TZM-bl cells suspended in cell culture medium were seeded into 96-well plates (1×10^4 cells/well) and into the wells of the PEDOT:PSS electrode arrays (3×10^4 cells/well) and were exposed to the Env HIV-1 IMC/inhibitor mixture. Luminescence values (RLU) measured 48 h after Env HIV-1 IMC virus/inhibitor exposure or area under the curve (AUC) for IZI_{norm} between 0 and 70 h were plotted against serial inhibitor dilutions to analyze IC_{50} values for TZM-bl cells using a four-parameter logistic fit (OriginPro2023). RLU: $n \geq 2$, AUC IZI_{norm}: $n \geq 4$, mean $\pm$ SEM. Values for the lowest antibody/drug concentration correspond to full virus load but no antibody/drug additives. Values for the highest antibody/drug concentration correspond to a virus-free control.

TABLE 2 | Comparison of results returned from impedance or firefly luciferase reporter gene readouts during exposure of TZM-bl host cells to two different Env HIV-1 IMCs (Ce1176 and X1632) in presence of two different *broadly neutralizing antibodies* (bnAB) or *non-nucleoside reverse transcriptase inhibitor* (NNRTI) Efavirenz (EFV). IC_{50} values of bnAB or NNRTI are given as mean $\pm$ SEM (impedance: $n \geq 4$, reporter gene expression: $n \geq 2$).

| | Virus Clone Ce1176 IC_{50} value | | Virus Clone X1632 IC_{50} value | |
| | bnAB CH31 (µg/mL) | NNRTI EFV (ng/mL) | bnAB 2F5 (µg/mL) | NNRTI EFV (ng/mL) |
Readout				
Impedance/PEDOT:PSS	2.2 ± 0.5	8 ± 7	9 ± 4	0.74 ± 0.11
Firefly luciferase expression	3.7 ± 0.4	0.25 ± 0.05	4.4 ± 0.7	0.16 ± 0.05

exposure. When clone Ce1176 was exposed to increasing concentrations of EFV, the reporter gene assay returned a typical dose–response relationship with an IC_{50} of (0.25 ± 0.05) ng/mL. The corresponding analysis of the impedance readout (AUC) did not yield a sigmoidal dose–response and quantification of IC_{50} is rather questionable. Formally, the analysis provided an IC_{50} of (8 ± 7) ng/mL. Besides the fact that this IC_{50} is significantly higher than the one determined from bioluminescence readouts, the shape of the dose–response curve indicates some unspecific toxicity of EFV/Ce1176 to the host cells that does not affect the expression of the reporter gene but induces cell death. We find support for this interpretation from the fact that the three highest concentrations of EFV reduce the AUC dose-dependently instead of converging with the AUC recorded for cells in the absence of viruses (final data point at the right end of the scale). This convergence is expected for compounds that inhibit viral infection without unspecific harmful effects on the host cells. Another possible explanation is a kind of cytotoxic effect on TZM-bl cells due to the high viral load used in impedance-based assays in combination with the well-known formation of syncytia in host cells induced by Env HIV-1 [43]. When clone X1632 was exposed to EFV, impedance and bioluminescence returned typical dose–response relationships and IC_{50} values were determined to (0.74 ± 0.11) ng/mL for impedance and (0.16 ± 0.05) ng/mL for the bioluminescence readout. Again, these values are statistically different but practically very similar, supporting our notion that impedance analysis using PEDOT:PSS electrodes has proven its suitability for these types of assays relative to reporter gene assays which are considered as the current gold standard.

However, looking at the well-to-well reproducibility of measurements recorded for one given experimental condition, as indicated by the standard deviation of the data points in the dose–response curves summarized in Figure 8, it is obvious that impedance readings show more data scattering. Putting a number to these hallmarks of cell-based assays, we calculated the Z' values according to Equation (1) for an impedance-based readout and compared it to Z' of the luminescence readout on the example of the dose–response relationship presented in Figure 8A:

$$Z' = 1 - \frac{3 \times (\sigma_p + \sigma_n)}{|\mu_p - \mu_n|},\tag{1}$$

Herein, μ_p and μ_n denote the average of the positive (p) and negative (n) control, respectively, while σ_p and σ_n stand for their standard deviations. Z' of an ideal assay is 1.0. Assays performing better than 0.5 are considered useful for high throughput screening (HTS) [44]. When we use the upper asymptotes of the dose–response relationships in Figure 8A as values for the positive control and the lower asymptotes for the corresponding negative controls, the calculation returns Z' values of 0.51 for the impedance-based analysis of the neutralization assay and 0.93 for the bioluminescence readout. These values clearly show that both readouts are suitable for HTS, but the bioluminescence assay has significantly better robustness. We can only speculate about the reasons for this observation. Whereas reporter gene assays are molecularly specific and only report on the activation of the promotor controlling the reporter

gene, impedance measurements are holistic in nature and integrate over the entire cell body and all stimulations affecting the cells at a given point in time – specific and unspecific. Differences in liquid handling, temperature gradients and slight differences in electrode geometry will contribute to the final readout, to mention just a few. These small but unspecific disturbances of the culture get mirrored in the impedance time courses. But we have experienced with other assays in the past, that further assay optimization addressing this particular issue will improve assay performance in the long-run. On the other hand, the example presented in Figure 8B shows the strength of this approach. The reporter gene assay is essentially blind to the unspecific toxicity that we observed in impedance readings (Figure 8B) which may be due to overdosing of EFV or an unspecific cell response due to the high virus load.

4 | Summary and Conclusion

A cost-effective impedance-based sensor platform for fully automated cell-based virological assays in 96-well format suitable for high throughput screening campaigns comprising hardware, software and disposable electrode arrays has been described in this study. To improve on cost-effectiveness of impedance-based readouts, we tested screen printed film electrodes made from the organic conducting polymer PEDOT:PSS prepared on the bottom of disposable multi-well plates. Besides impedance electrodes, electrical connections and passivation layer were screen printed as well, allowing low-cost reel-to-reel production of disposable electrode arrays. The polymer electrodes were shown to be host cell compatible and the integral sensitivity of PEDOT:PSS for cell-based impedance measurements was found to be better in comparison to established gold-film electrodes. Hard- and software were tailored for robust and routine use in virological assays. The sensor platform showed a higher sensitivity for lytic (VSV) compared to non-lytic viruses (HIV). The former destroy cell structure upon infection through the CPE, while the latter just affect cells via CPE that does not result in massive cell shape changes. Virus titration, virus neutralization and antiviral drug intervention assays showed very similar analytical performances in terms of titration curves and dose–response relationships for PEDOT:PSS electrodes compared to both, commercial gold-film electrodes and reporter-based endpoint assays. In summary, the disposable PEDOT:PSS electrodes offer great potential to compete with classical/established readouts of cell-based virological assays due to low manufacturing costs by replacing expensive electrode materials such as gold or platinum. Moreover, the sensor platform is transferable to other assay formats beyond virological problems. Besides a fully automated, label-free and time-resolved readout of virological assays, the novel impedance platform may also be applied for a variety of impedance-based phenotypic assays with high temporal resolution in the future without further development, like monitoring of cell receptor stimulation and cell signaling (G-protein coupled receptors, GPCRs), drug screening or toxicological in vitro studies. Overall, the low-cost polymer electrode arrays may become an attractive alternative to conventional gold-film electrode arrays.

Conflicts of Interest

S.M., A.G., A.K.M., I.R., S.B., T.K., S.W. and J.W. declare no conflict of interest. J.J., E.K. and D.B. have been employees of innoMe GmbH at the time when this study was conducted. Neither one of them is still working for innoMe GmbH today. M.S. and B.A. are affiliated with nanoAnalytics GmbH. The company produces and sells impedance platforms by the tradename cellZscope for use in cell-based assays.

Data Availability Statement

The data that support the findings of this study are available from the corresponding author upon reasonable request.

References

1. A. E. Muruato, C. R. Fontes-Garfias, P. Ren, et al., "A High-Throughput Neutralizing Antibody Assay for COVID-19 Diagnosis and Vaccine Evaluation," *Nature Communications* 11 (2020): 4059.

2. C. Chen, J. Liang, H. Hu, X. Li, L. Wang, and Z. Wang, "Research Progress in Methods for Detecting Neutralizing Antibodies Against SARS-COV-2," *Analytical Biochemistry* 673 (2023): 115199.

3. J. R. Izac, E. J. Kwee, L. Tian, et al., "Development of a Cell-Based SARS-CoV-2 Pseudovirus Neutralization Assay Using Imaging and Flow Cytometry Analysis," *International Journal of Molecular Sciences* 24, no. 15 (2023): 12332.

4. R. Kalkeri, Z. Cai, S. Lin, J. Farmer, Y. V. Kuzmichev, and F. Koide, "SARS-CoV-2 Spike Pseudoviruses: A Useful Tool to Study Virus Entry and Address Emerging Neutralization Escape Phenotypes," *Microorganisms* 9, no. 8 (2021): 1744.

5. J. Bi, H. Wang, H. Pei, et al., "A Novel and Secure Pseudovirus Reporter System Based Assay for Neutralizing and Enhancing Antibody Assay Against Marburg Virus," *Frontiers in Microbiology* 13 (2022): 927122.

6. J. Nie, Q. Li, J. Wu, et al., "Quantification of SARS-CoV-2 Neutralizing Antibody by a Pseudotyped Virus-Based Assay," *Nature Protocols* 15 (2020): 3699–3715.

7. B. J. Cohen, D. Doblas, and N. Andrews, "Comparison of Plaque Reduction Neutralisation Test (PRNT) and Measles Virus-Specific IgG ELISA for Assessing Immunogenicity of Measles Vaccination," *Vaccine* 26, no. 50 (2008): 6392–6397.

8. M. Sarzotti-Kelsoe, R. T. Bailer, E. Turk, et al., "Optimization and Validation of the TZM-bl Assay for Standardized Assessments of Neutralizing Antibodies Against HIV-1," *Journal of Immunological Methods* 409 (2014): 131–146.

9. D. C. Montefiori, "Measuring HIV Neutralization in a Luciferase Reporter Gene Assay." in *HIV Protocols. Methods in Molecular Biology*, eds. V. R. Prasad and G. V. Kalpana, 2009. 485, 395–405.

10. Clinical Immunology (2019): Elsevier.

11. S. Lukic and J. Wegener, "Impedimetric Monitoring of Cell-Based Assays," *eLS*: 1–8 (2015).

12. B. Freiesleben De Blasio and J. Wegener, "Impedance Spectroscopy," in *Encyclopedia of Medical Devices and Instrumentation*, ed. J. G. Webster, 2nd edition (2006), 132–144.

13. J. Wegener, "Tierische Zellen als Sensoren zur Bioaktivitätsprüfung: Effekt- Statt Konzentrationsanalytik mit Label-Freien Methoden," *Blick in die Wissenschaft* 22, no. 27 (2013): 19–23.

14. J. Wegener, C. R. Keese, and I. Giaever, "Electric Cell-Substrate Impedance Sensing (ECIS) as a Noninvasive Means to Monitor the Kinetics of Cell Spreading to Artificial Surfaces," *Experimental Cell Research* 259, no. 1 (2000): 158–166.

15. S. Michaelis and J. Wegener, "Zellen als Sensoren." in *Biologische Transformation*, eds. R. Neugebauer (Berlin, Heidelberg: Springer Berlin Heidelberg, 2019), 109–132).

16. A. Janshoff, A. Kunze, S. Michaelis, V. Heitmann, B. Reiss, and J. Wegener, "Cell Adhesion Monitoring Using Substrate-Integrated Sensors," *Journal of Adhesion Science and Technology* 24 (2010): 2079–2104.

17. C. R. Keese, J. Wegener, S. R. Walker, and I. Giaever, "Electrical Wound-Healing Assay for Cells In Vitro," *Proceedings of the National Academy of Sciences* 101, no. 6 (2004): 1554–1559.

18. R. Szulcek, H. J. Bogaard, and G. P. van Nieuw Amerongen, "Electric Cell-Substrate Impedance Sensing for the Quantification of Endothelial Proliferation, Barrier Function and Motility," *Journal of visualized experiments: JoVE* no. 85 (2014): 51300.

19. F. Asphahani and M. Zhang, "Cellular Impedance Biosensors for Drug Screening and Toxin Detection," *Analyst* 132, no. 9 (2007): 835–841.

20. D. Opp, B. Wafula, J. Lim, E. Huang, J.-C. Lo, and C.-M. Lo, "Use of Electric Cell-Substrate Impedance Sensing to Assess In Vitro Cytotoxicity," *Biosensors and Bioelectronics* 24, no. 8 (2009): 2625–2629.

21. M. Zinkl and J. Wegener, "Using Animal Cells as Sensors for Xenobiotics: Monitoring Phentotypic Changes by Multimodal Impedance Assays," *Current Opinion in Environmental Science & Health* 10 (2019): 30–37.

22. L. D. Robilliard, D. T. Kho, R. H. Johnson, A. Anchan, S. J. O'Carroll, and E. S. Graham, "The Importance of Multifrequency Impedance Sensing of Endothelial Barrier Formation Using ECIS Technology for the Generation of a Strong and Durable Paracellular Barrier," *Biosensors* 8, no. 3 (2018): 64.

23. S. Cho, S. Becker, H. von Briesen, and H. Thielecke, "Impedance Monitoring of Herpes Simplex Virus-Induced Cytopathic Effect in Vero Cells," *Sensors and Actuators B: Chemical* 123 (2007): 978–982.

24. Y. Fang, P. Ye, X. Wang, X. Xu, and W. Reisen, "Real-Time Monitoring of Flavivirus Induced Cytopathogenesis Using Cell Electric Impedance Technology," *Journal of Virological Methods* 173, no. 2 (2011): 251–258.

25. M. R. Pennington and G. R. Van de Walle, "Electric Cell-Substrate Impedance Sensing to Monitor Viral Growth and Study Cellular Responses to Infection with Alphaherpesviruses in Real Time," *mSphere* 2, no. 2 (2017), https://doi.org/10.1128/msphere.00039-17.

26. A.-K. Mildner, Development of an Impedance-Based Neutralization Assay for SARS-CoV-2 Infection With Inherent Amplification, *Master Thesis University of Regensburg* (2021).

27. E. Wintermantel and S.-W. Ha, *Medizintechnik - Life Science Engineering* (Springer Berlin Heidelberg, 2008).

28. A. S. Karimullah, D. R. S. Cumming, M. Riehle, and N. Gadegaard, "Development of a Conducting Polymer Cell Impedance Sensor," *Sensors and Actuators B: Chemical* 176 (2013): 667–674.

29. M. Dietrich, J. Heinze, G. Heywang, and F. Jonas, "Electrochemical and Spectroscopic Characterization of Polyalkylenedioxythiophenes," *Journal of Electroanalytical Chemistry* 369, no. 1–2 (1994): 87–92.

30. L. Groenendaal, F. Jonas, D. Freitag, H. Pielartzik, and J. R. Reynolds, "Poly(3,4-ethylenedioxythiophene) and Its Derivatives: Past, Present, and Future," *Advanced Materials* 12, no. 7 (2000): 481–494.

31. U. Leute, *Elektrisch leitfähige Polymerwerkstoffe* (Wiesbaden: Springer Fachmedien Wiesbaden, 2015), 1. Auflage, Buch IX.

32. E. J. Platt, K. Wehrly, S. E. Kuhmann, B. Chesebro, and D. Kabat, "Effects of CCR5 and CD4 Cell Surface Concentrations on Infections by Macrophagetropic Isolates of Human Immunodeficiency Virus Type 1," *Journal of Virology* 72, no. 4 (1998): 2855–2864.

33. X. Wei, J. M. Decker, H. Liu, et al., "Emergence of Resistant Human Immunodeficiency Virus Type 1 in Patients Receiving Fusion Inhibitor (T-20) Monotherapy," *Antimicrobial Agents and Chemotherapy* 46, no. 6 (2002): 1896–1905.

34. E. T. McAdams, A. Lackermeier, J. A. McLaughlin, D. Macken, and J. Jossinet, "The Linear and Non-Linear Electrical Properties of the Electrode-Electrolyte Interface," *Biosensors and Bioelectronics* 10, no. 1–2 (1995): 67–74.

35. I. Podolak, A. Galanty, and D. Sobolewska, "Saponins as Cytotoxic Agents: A Review," *Phytochemistry Reviews* 9 (2010): 425–474.

36. P. Pütz, A. Behrent, A. J. Baeumner, and J. Wegener, "Laser-Scribed Graphene (LSG) as New Electrode Material for Impedance-Based Cellular Assays," *Sensors & Actuators B: Chemical* 321 (2020): 128443.

37. Y. Gao and I. Bergman, "Vesicular Stomatitis Virus (VSV) G Glycoprotein Can Be Modified to Create a Her2/Neu-Targeted VSV That Eliminates Large Implanted Mammary Tumors," *Journal of Virology* 97, no. 6 (2023): e0037-2-23, https://doi.org/10.1128/jvi.00372-23.

38. S. A. Kopecky and D. S. Lyles, "Contrasting Effects of Matrix Protein on Apoptosis in HeLa and BHK Cells Infected with Vesicular Stomatitis Virus Are Due to Inhibition of Host Gene Expression," *Journal of Virology* 77, no. 8 (2003): 4658–4669.

39. M. Hoffmann, Y.-J. Wu, M. Gerber, et al., "Fusion-Active Glycoprotein G Mediates the Cytotoxicity of Vesicular Stomatitis Virus M Mutants Lacking Host Shut-Off Activity," *Journal of General Virology* 91, no. 11 (2010): 2782–2793.

40. P. Gadaleta, M. Vacotto, and F. Coulombié, "Vesicular Stomatitis Virus Induces Apoptosis at Early Stages in the Viral Cycle and Does Not Depend on Virus Replication," *Virus Research* 86, no. 1–2 (2002): 87–92.

41. A. K. Mildner, S. Einhauser, S. Michaelis, K. R. Bieberstein, R. Wagner, and J. Wegener, "Impedance-Based Monitoring of Titration and Neutralization Assays With VSV-G and SARS-CoV-2-spike Pseudoviruses," *Applied Research* 3, no. 1 (2024): e202400097.

42. T. G. Edmonds, H. Ding, X. Yuan, et al., "Replication Competent Molecular Clones of HIV-1 Expressing *Renilla luciferase* Facilitate the Analysis of Antibody Inhibition in PBMC," *Virology* 408, no. 1 (2010): 1–13.

43. M. Symeonides, T. Murooka, L. Bellfy, N. Roy, T. Mempel, and M. Thali, "HIV-1-induced Small T Cell Syncytia Can Transfer Virus Particles to Target Cells Through Transient Contacts," *Viruses* 7, no. 12 (2015): 6590–6603.

44. J.-H. Zhang, T. D. Y. Chung, and K. R. Oldenburg, "A Simple Statistical Parameter for Use in Evaluation and Validation of High Throughput Screening Assays," *SLAS Discovery* 4, no. 2 (1999): 67–73.

Supporting Information

Additional supporting information can be found online in the Supporting Information section.